



## Original Article

## Hybrid medium model for conjugate heat transfer modeling in the core of sodium-cooled fast reactor



X.A. Wang, Dalin Zhang<sup>\*</sup>, Mingjun Wang, Ping Song, Shibao Wang, Yu Liang, Yapei Zhang, Wenxi Tian, Suizheng Qiu, G.H. Su

School of Nuclear Science and Technology, Shaanxi Key Laboratory of Advanced Nuclear Energy and Technology, State Key Laboratory of Multiphase Flow in Power Engineering, Xi'an Jiaotong University, Xi'an, 710049, China

## ARTICLE INFO

## Article history:

Received 3 May 2019

Received in revised form

12 August 2019

Accepted 19 September 2019

Available online 22 September 2019

## Keywords:

Porous medium model

Hybrid medium model

Conjugate heat transfer

Inter-wrapper flow

Sodium-cooled fast reactor

## ABSTRACT

Core-wide temperature distribution in sodium-cooled fast reactor plays a key role in its decay heat removal process, however the prediction for temperature distribution is quite complex due to the conjugate heat transfer between the assembly flow and the inter-wrapper flow. Hybrid medium model has been proposed for conjugate heat transfer modeling in the core. The core is modeled with a Realistic modeled inter-wrapper flow and hybrid medium modeled assembly flow. To validate present model, simulations for a three-assembly model were performed with Realistic modeling, traditional porous medium model and hybrid medium model, respectively. The influences of Uniform/Non-Uniform power distribution among assemblies and the Peclet number within the assembly flow have been considered. Compared to traditional porous medium model, present model shows a better agreement with in Realistic modeling prediction of the temperature distribution and the radial heat transfer between the inter-wrapper flow and the assembly flow.

© 2019 Korean Nuclear Society, Published by Elsevier Korea LLC. This is an open access article under the CC BY-NC-ND license (<http://creativecommons.org/licenses/by-nc-nd/4.0/>).

## 1. Introduction

For the design and safety purpose, core-wide thermal-hydraulic simulation for sodium-cooled fast reactors (SFR) need to be performed [1]. The pool-type sodium-cooled fast reactor is famous for its passive safety characteristic where the decay heat in the core can be removed from the core by the natural circulation within the sodium pool even under the unprotected accident conditions. During the passive heat removal process, flow within the assembly is driven by buoyancy force which is sensitive to the exact temperature distribution within each assembly of the core [2]. In addition, the influence of inter-wrapper flow (IWF) is quite significant due to the large flow rate and strong heat exchange with the assembly flow during the decay heat removal process, as demonstrated by experiments [3,4]. Core-wide thermal-hydraulic simulation requires a full-core model that consists of fuel assemblies and inter-assembly gaps. However, due to the large dimension difference between the fuel assembly (in 100 mm order) and the inter-assembly gap (in several mm order), it is prohibitively expensive

to model the whole core with the Realistic modeling method that represents the geometry of fuel rod within the assembly [5].

In order to reduce the computational cost, several simplified resolution methods have been proposed for the whole modeling in the past few decades. The most widely used approach is modeling the reactor core with subchannel codes that represent the assembly flow (AF) and the inter-wrapper flow (IWF) with 1D parallel channels. A sub-channel analysis code SUPERENERGY-2 was developed for SFR analysis based on the experiments of wire-wrapped fuel rod bundles with liquid sodium by MIT and Pacific Northwest National Laboratory. Due to the simplification of central channels, it is less computational cost compared to traditional subchannel codes [6,7]. The subchannel model in AQUA was managed to model the whole core with low computational cost by transforming the hexagon geometry of assembly into rectangle [8]. Recently, a similar code SAM was developed at Argonne National Laboratory (ANL), which was reported holding the ability for 3D full core conjugate heat transfer modeling analysis [9]. This type approach is able for quotidian analyses with very limited computational cost. However, it is very cumbersome to obtain the detail information about such temperature fluctuation within the assembly flow (AF), the inter-wrapper flow (IWF) and the duct, which is important for local flow field analysis and thermal-mechanical

<sup>\*</sup> Corresponding author.

E-mail address: [dlzhang@mail.xjtu.edu.cn](mailto:dlzhang@mail.xjtu.edu.cn) (D. Zhang).

analysis. To improve the simulation, French Alternative Energies and Atomic Energy Commission (CEA) developed a multi-level full-core model through a coupling of a subchannel model for the assembly flow and a 3D CFD model for the inter-wrapper flow within TRIO\_U software [10].

With the maturity of computational fluid dynamic (CFD) method, some researchers turned to porous medium approach. A 3D CFD model for the primary of the PFBR by Parthasarathy et al. for the analysis of decay heat removal process [11]. The core was modeled with uniform porous medium for the assembly flow and realistic model for the inter-wrapper flow. However, the later research conducted by Yu [12] shows that the uniform porous medium model will result in an overestimation of the duct wall seriously. Fuel rods have a looser packing near the surface of duct within AF comparing to the bulk. Larger porosity near the wall will cause a lower volumetric heat source and a larger velocity distribution, which has a great influence for the radial heat transfer between the assembly flow and the inter-wrapper flow.

Different to general porous medium where the packed particles contact the duct wall directly, all rods in SFR fuel assembly do not contact the duct wall. In other words, there exists a pure fluid layer near the duct wall in SFR fuel assemblies. Therefore, the assembly flow could be divided into a porous region immersed with fuel rods in the center and a pure fluid region filled with coolant in the peripheral. This configuration is so called hybrid medium. Several researchers have applied this method to the simulation of forced flows in composite channels consisting of a porous layer and a pure fluid layer [13–15].

This paper studied the applicability of hybrid medium model as well as two conventional porous medium model for the fuel assembly of SFR. A three-assembly model including the inter-wrapper flow was developed as a simplified model of the whole. Both Realistic modeling method and porous medium methods were applied for the temperature distribution within AF and IWF as well as the radial heat transfer between AF and IWF. Comparing with conventional porous medium model, hybrid medium model is able to predict the radial temperature distribution at the core outlet well, especially for the inter-wrapper flow.

## 2. Model description

### 2.1. CFD model

A three-fuel assembly model has developed to examine porous medium methods for conjugate heat transfer in Fluent. The fuel assembly geometry comes from China Experimental Fast Reactor(CEFR) [16], the major parameters of which are listed in Table 1. The assembly has a relative small coolant flow area with  $P/D$  of 1.17.

For simplicity, the bar fuel rod assembly is consideration in present research, as shown in Fig. 1. The same inlet boundary

**Table 1**  
CEFR fuel assembly geometry.

Assembly parameters	Value
Pin number (N)	61
Assembly pitch(mm)	61.00
Duct inner flat-to-flat distance (mm)	56.60
Duct outside flat-to-flat distance (mm)	61.00
Duct thickness(mm)	1.20
Inter-wrapper gap width(mm)	2.00
Assembly Length(mm)	1350.00
<b>Pin parameters</b>	
Pin diameter $D_r$ (mm)	6.00
Pin pitch $P$ (mm)	7.00

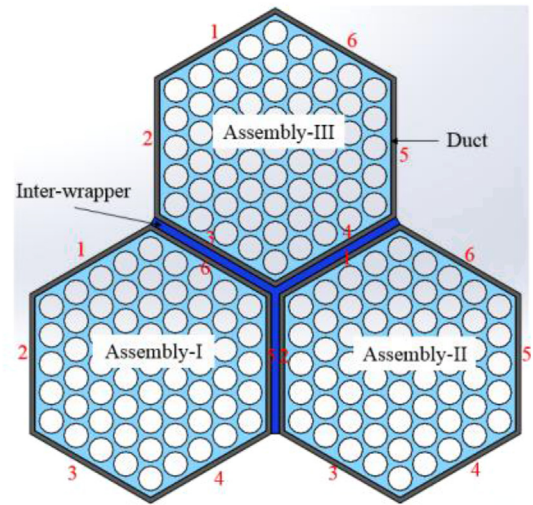


**Fig. 1.** Three-fuel assembly model.

condition (both flow rate and temperature) is applied for all assemblies. IWF takes the same temperature at the inlet but with a smaller inlet velocity. Power distribution within each assembly is assumed both in radial and axial direction, as listed in Table 2. Two thermal modes are considered. In the first one, a uniform power distribution is assumed among three assemblies where fuel rods hold the same surface heat flux. In the second one, a non-uniform power distribution is assumed among three assemblies. Duct walls without contact with IWF are assumed adiabatic.

The material for coolant and duct are liquid sodium and Zircaloy, respectively. Their thermal properties all keep constant in this work, as listed in Table 3.

### 2.2. Porous medium model

The macroscopic governing equations for flow through a porous medium can be obtained through volume averaging. For incompressible fluid with constant properties, the governing equation for momentum in porous medium could be present as follows:

**Table 2**  
Boundary conditions.

Parameters	AF	IWF
Inlet velocity (m/s)	1.50–7.00	0.1
Inlet temperature(K)	636.0	636.0
Outlet pressure(Pa)	0.0	0.0
Heat flux(W /m <sup>2</sup> )(Uniform power)	Assembly-I	$2.0 \times 10^5$
	Assembly-II	$2.0 \times 10^5$
	Assembly-III	$2.0 \times 10^5$
Heat flux(W /m <sup>2</sup> )(Non- Uniform power)	Assembly-I	$2.0 \times 10^5$
	Assembly-II	$2.5 \times 10^5$
	Assembly-III	$1.5 \times 10^5$

**Table 3**  
Thermal properties for materials.

Parameters	Liquid sodium	Zircaloy
Density (kg /m <sup>3</sup> )	846	6570
Specific heat capacity (J /K/kg)	1273	336.13
Thermal conductivity (W /K/m)	65	13.22
Dynamic viscosity (Pa·s)	0.000264	–

$$\frac{\partial \gamma \rho \bar{u}_i}{\partial t} + \frac{\partial}{\partial x_j} (\gamma \rho \bar{u}_i \bar{u}_j) = -\frac{\partial}{\partial x_i} (\gamma p) + \frac{\partial}{\partial x_j} [\gamma (\mu_{Lam} + \mu_{Tur}) (\frac{\partial u_i}{\partial x_j} + \frac{\partial u_j}{\partial x_i})] + \gamma f_i \quad (1.1)$$

Where  $\gamma$  is the volume porosity, and  $f_i$  stands for the body force caused by friction on the fuel rod surface.

$$f_i = f \frac{\rho |\vec{u}| u_i}{2D_e} \quad (1.2)$$

Where  $f$  is the friction coefficient. According to the research conducted by Rehme [17], the friction factor for triangular rod bundles could be decided with following correlations:

For  $Re = 10^4$ :

$$\frac{f}{f_{c,t}} = 1.045 + 0.071 \left( \frac{P}{D} - 1 \right) \quad (1.3)$$

For  $Re = 10^5$ :

$$\frac{f}{f_{c,t}} = 1.036 + 0.054 \left( \frac{P}{D} - 1 \right) \quad (1.4)$$

Where  $f_{c,t}$  is the circular tube friction factors.

Reynolds number	Friction coefficient
$Re_D < 30000$	$f_{c,t} = 0.316 Re^{-0.25}$
$30000 < Re_D < 1000000$	$f_{c,t} = 0.184 Re^{-0.2}$

For turbulence model, two equation model  $k-\epsilon$  is adopted. According to the published research [15], macroscopic governing equations for turbulence kinetic energy and dissipation rate could be decided as follows:

$$\frac{\partial \gamma \rho k}{\partial t} + \frac{\partial}{\partial x_i} (\gamma \rho \bar{u}_i k) = \frac{\partial}{\partial x_j} [\gamma (\mu_{Lam} + \frac{\mu_{Tur}}{\sigma_k}) \frac{\partial k}{\partial x_j}] + \mu_{Tur} S^2 \nabla \bar{u}_i + c_k \rho \frac{k |\bar{u}_i|}{\sqrt{K}} - \gamma \rho \epsilon \quad (1.5)$$

$$\frac{\partial \gamma \rho \epsilon}{\partial t} + \frac{\partial}{\partial x_i} (\gamma \rho \bar{u}_i \epsilon) = \frac{\partial}{\partial x_j} [\gamma (\mu_{Lam} + \frac{\mu_{Tur}}{\sigma_\epsilon}) \frac{\partial \epsilon}{\partial x_j}] + C_{1\epsilon} \mu_{Tur} S^2 \nabla \bar{u}_i \frac{\epsilon}{K} + C_{2\epsilon} \rho \{ c_k \rho \frac{k |\bar{u}_i|}{\sqrt{K}} - \gamma \frac{\epsilon^2}{K} \} \quad (1.6)$$

Where  $\sigma_k = 1.0$ ,  $\sigma_\epsilon = 1.3$ ,  $c_k = 0.28$ ,  $K$  is the medium permeability. According to the research for packed beds with circular tube [18], the medium permeability is decided as follows:

$$K = \frac{D^2 \gamma^3}{140(1 - \gamma)^2} \quad (1.7)$$

By solving the heat conduction equation  $\nabla T^2 = 0$  in triangular rod bundle configuration, an anisotropy effective heat conductivity could be obtained. Therefore, the macroscopic governing equation for energy could be expressed as:

$$[\gamma (\rho c_p)_f] \frac{\partial T}{\partial t} + \gamma (\rho c_p)_f \nabla \cdot (\bar{u} T) = \nabla \cdot (k_{eff} \nabla T) \quad (1.8)$$

Where  $k_{eff}$  is the effective heat transfer tensor:

$$\begin{cases} k_{eff,r} = (\kappa \frac{c_{pf} \mu_t}{Pr_t} + \kappa k_f) + k_{disp} \\ k_{eff,z} = (\gamma \frac{c_{pf} \mu_t}{Pr_t} + \gamma k_f) + k_{disp} \end{cases} \quad (1.9)$$

Where  $\kappa = (1 - \frac{D}{P})$  is the tortuosity in the open literature,  $D$  is rod diameter,  $P$  is rod pitch [6],  $Pr_t$  is the turbulent Prandtl number. According to the public research, the turbulence Prandtl number and wall turbulence Prandtl number are modified from 0.85 to 1.5.  $k_{disp}$  is the thermal dispersion tensor. According to the work of Lemos [19], the thermal dissipation tensor for bar rod fuel assembly could be decided with following correlation.

$$k_{disp,r} = 1.55 \times 10^{-4} Pe_p^{0.94} k_f \quad (1.10)$$

Where  $Pe_p = U_z P / \alpha$ ,  $\alpha$  is the thermal diffusivity.

Three porous medium models are studied in this paper. In the first porous medium model, AF is taken as one porous medium region with uniform porosity and uniform volumetric heat flux. The porosity is decided based on the ratio of fluid volume in real model region to total volume of porous medium. The second porous medium model divides the AF into two regions with the line joining the centers of the peripheral rods. And different porosities and volumetric heat fluxes are set for two regions, respectively.

In third porous medium model, the AF is divided into two regions with a hexagon box that is large enough to contain all fuel rods. Supposing the across flat width of the hexagon box is  $W$ . Assuming the porosity is uniform in central-region and it equals to that in central-channel.

$$1 - \frac{\sqrt{3} \pi D^2}{6P^2} = 1 - \frac{\sqrt{3} N \pi D^2}{6W^2} \quad (1.11)$$

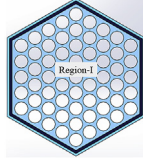
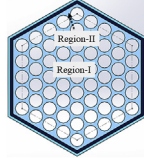
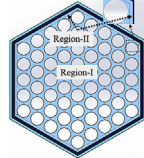
Where  $(1 - \frac{\sqrt{3} \pi D^2}{6P^2})$  is the porosity for central channel,  $(1 - \frac{\sqrt{3} N \pi D^2}{6W^2})$  is the porosity for central region in the hexagon box.  $N$  is are fuel rod number.

The across flat width  $W$  could be determined by  $W = \sqrt{NP}$ , and it is smaller than the across flat width of the assembly. Further analysis shows that parameters such as volumetric heat source, fuel wall surface area density and hydraulic diameter in Region-I are the same with those corresponding in of central-channels, respectively. Key parameters for Region-I in three porous medium models are listed Table-4.

### 2.3. Solving algorithms

Based on the verification study of the turbulence model [21], the realizable  $k-\epsilon$  turbulence model is employed. Near the wall, two-layer all  $y^+$  wall function is adopted. Since the Reynold number for IWF is lower than the critical number (2300), turbulence model has been suppressed with laminar choice in Fluent. The convection term in transport equations all take second order upwind discretization scheme. The interpolation scheme for pressure takes PRESTO!, which is similar to the stagger-grid schemes used with structured meshes in principle. Segregated flow solver and the SIMPLE predictor corrector algorithm. The simulation is converged as the normalized residuals are below  $10^{-4}$ .

**Table 4**  
Key parameters for Region-I.

Parameters	Model-1	Model-2	Model-3
Across flat width(mm)	56.60	48.50	54.67
Volume Porosity( $\gamma$ )	0.38	0.33	0.33
Volumetric Heat source( $Q$ )	$\frac{2N\pi d}{\sqrt{3}F^2}q$	$\frac{2\pi d}{\sqrt{3}p^2}q$	$\frac{2\pi d}{\sqrt{3}p^2}q$
Hydraulic diameter( $De$ )	$\frac{2\sqrt{3}p^2}{\pi d} - d$	$\frac{2\sqrt{3}p^2}{\pi d} - d$	$\frac{2\sqrt{3}p^2}{\pi d} - d$
Region Sketch			

#### 2.4. Mesh sensitivity analysis

The meshing software “Meshing” by ANSYS Inc is employed to build mesh models for Realistic modeling and porous medium models, as shown in Fig. 2.

According to the suggestion from the BPG [20], a mesh model with 22.2 million cells was built for Realistic modeling. 7 nodes are assigned for the inter-wrapper gap, 3 nodes are assigned for the duct wall and the radial-to-axial aspect ratio is 1:10. To verify the realistic model, the friction factors predicted by the realistic model and experimental correlations were compared for the assembly flow, as shown in Table 5. It could be observed that the friction factors predicted by different models are quite close and the biggest relative deviation is not larger than 3%.

For porous medium model, Model-3 holds the highest requirement for mesh density among three porous medium model due to the existence of the pure fluid layer near the wall. Therefore, Model-3 is employed for the mesh sensitivity study. Node assignments stay the same as in Realistic modeling for the inter-wrapper gap and duct wall. The detailed parameters for the mesh sensitivity study are listed in Table 6, where  $b$  stands for radial nodes in region-II. Fig. 3 shows the total surface heat transfer across wall-6 of Assembly-I with different mesh models. It is found that when  $a = 12$ ,  $b = 4$ ,  $c = 450$ , the total surface heat transfer is independent from mesh model approximately. Accordingly, the mesh model contains a total cell number of 1 045 800.

### 3. Results and discussion

Three models are employed to predict the radial heat transfer between IWF and AF. The results are compared with those from the Realistic modeling.

#### 3.1. Uniform power distribution

##### 3.1.1. Results at a given Peclet number = 174

Fig. 4 shows the temperature distribution contour predicted by different models at the outlet of assemblies. Due to the channel effect that axial velocity near duct wall is higher than that in the central region, more energy is taken away near the wall. Temperature near the duct wall is lower than that in central region, i.e., temperature should decrease along radial direction within AF. Realistic modeling produces the temperature distribution as expected. But Model-1 shows a different temperature distribution that increases along the radial direction, as shown in Fig. 4(b). It is because the non-slip assumption on the duct wall imposes extra shear stress to fluid near the wall, which results in the axial velocity in the near wall region is lower than that in central region. Since the fluid with lower velocity takes away less energy, the temperature in the near wall region is higher than that in the central region. Moreover, the shear stress at the corner is higher than that along the flat wall which results in much lower velocity distribution. Therefore, the corner region holds the highest temperature

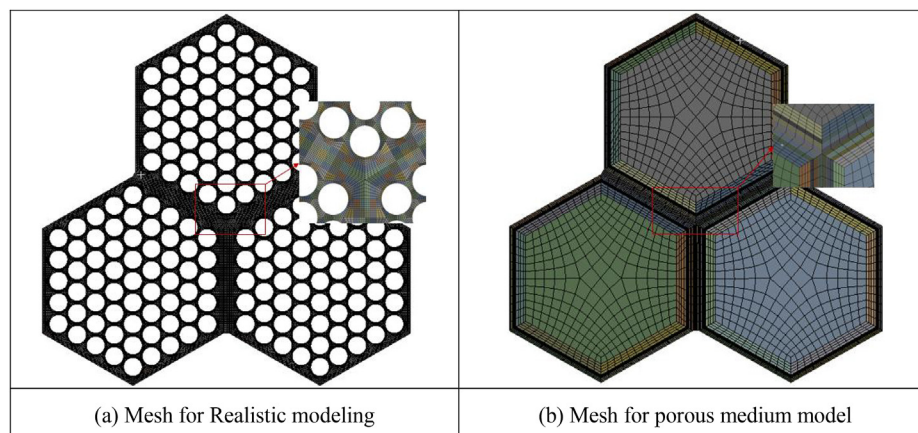


**Fig. 2.** Mesh models for Realistic modeling and porous medium model.

**Table 5**  
Comparison of predicted friction factor.

Reynold number	Predicted friction factor $f$		
	By correlations	By the realistic model	Relative deviation (%)
28889	0.0242	0.0249	2.84
33704	0.0233	0.0237	1.74
43334	0.0219	0.0220	0.38
52964	0.0208	0.0209	0.20
67408	0.0196	0.0197	0.25

**Table 6**  
Mesh parameters for sensitivity study.

Mesh in axial direction					Mesh in Circumference direction					Mesh in radial direction				
#	$a$	$b$	$c$	Cell number	#	$a$	$b$	$c$	Cell number	#	$a$	$b$	$c$	Cell number
1	12	4	135	152 820	5	6	4	450	509 400	9	12	1	450	851 400
2	12	4	270	419 949	6	12	4	450	778 950	10	12	2	450	916 200
3	<b>12</b>	4	450	486 900	7	18	4	450	1050 750	<b>11</b>	<b>12</b>	<b>4</b>	<b>450</b>	<b>1045 800</b>
4	12	4	1350	1505 250	8	24	4	450	1321 200	12	12	6	450	1175 400

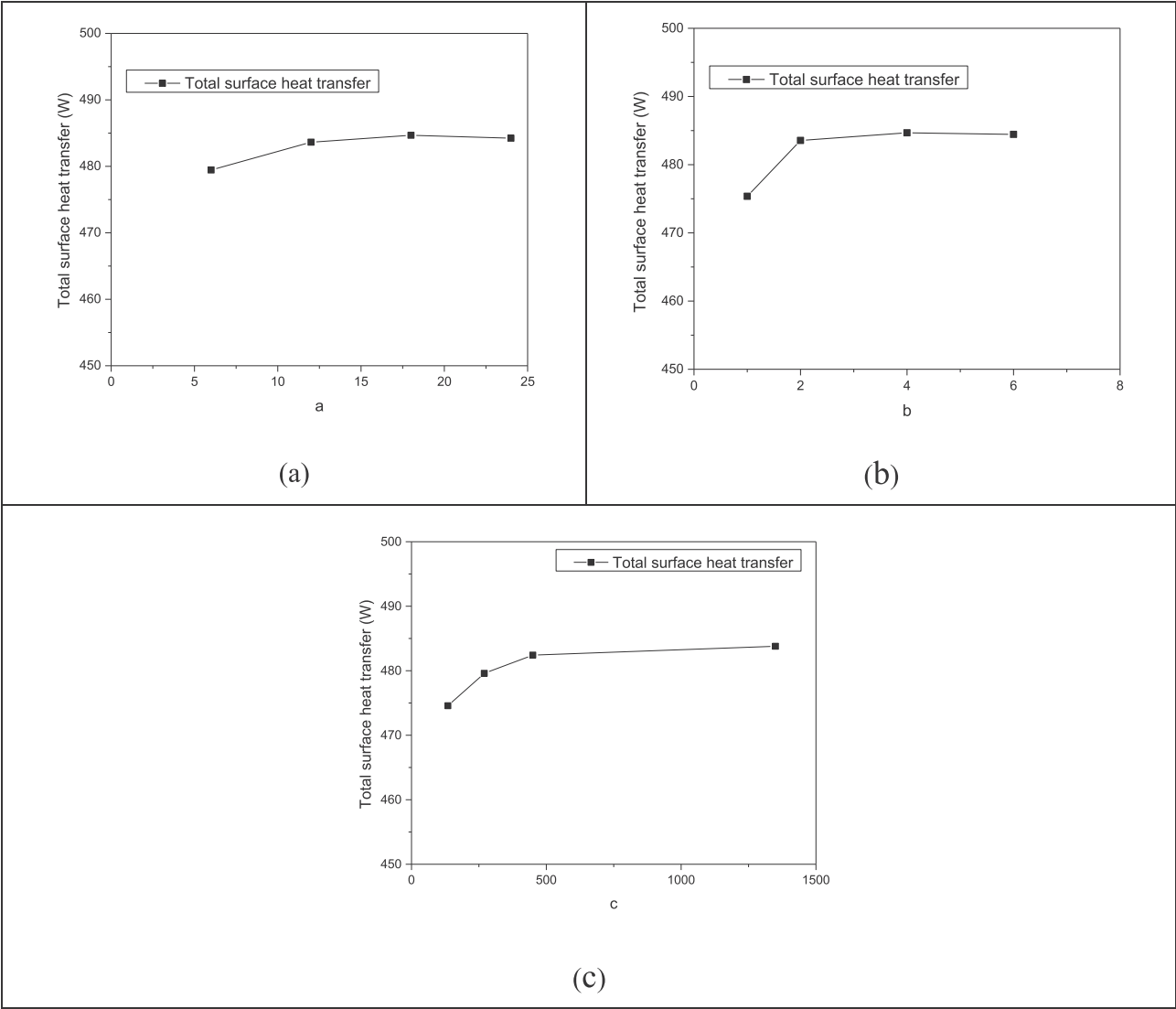


**Fig. 3.** Mesh sensitivity study for porous medium Model-3.



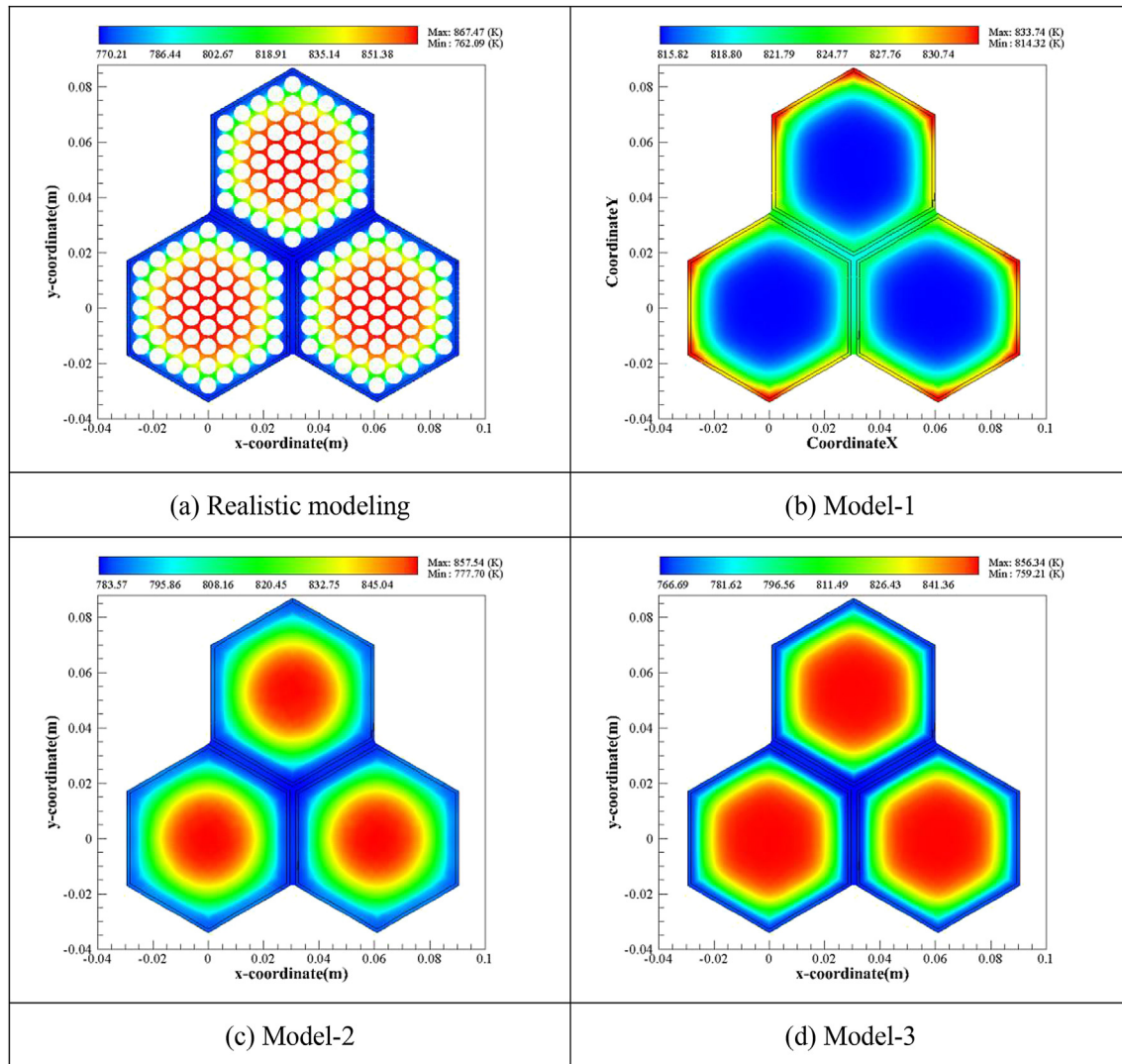


Fig. 4. Temperature at the outlet of AF (Uniform power distribution).

distribution. Due to the radial heat transfer between AF and IWF, some corners show a smaller temperature than the rest. However, radial heat transfer did not eliminate the wrong radial temperature distribution within AF predicted by Model-1. The temperature distribution within AF plays an important role in the radial heat transfer prediction between AF and IWF, the uniform porous medium model may could not be used for the conjugate heat transfer prediction in SFR core.

Model-2 and Model-3 reproduced the radial temperature distribution with some deviation for the exact temperature value. In particular, Model-2 over predict the minimum temperature by a deviation of about 16K, while model-3 underestimate the minimum temperature by a deviation of about 2.9K. The over-prediction of Model-2 may be caused by an artificial of volumetric heat flux distribution in the very vicinity of the duct wall, which is not existed in the real model. As in model-1, the artificial of volumetric heat flux distribution may result in a higher temperature distribution near the duct inside wall. Consequently, the IWF temperature is overestimated though radial heat conduction.

Both of Model-2 and Model-3 underestimate the maximum temperature in the central region by a deviation of about 10K. This underestimation could be explained by an overestimation of flow in the center region. For AF, the boundary layer in porous medium

model is thicker than that in real model due to the lack of confinement from fuel rods. In porous medium model, coolant tends to flow in the central region, which will take more energy from the center region. Therefore, the highest temperature in central region predicted by porous medium model is lower than the real model. To confirm this explanation, one assembly is divided

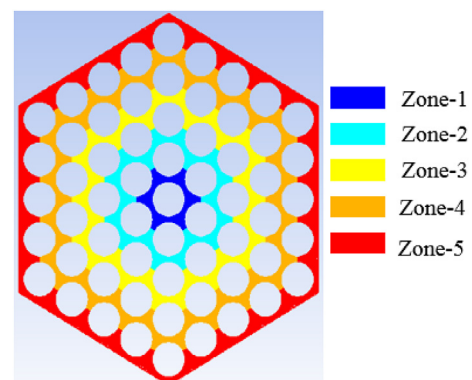


Fig. 5. Division of the AF

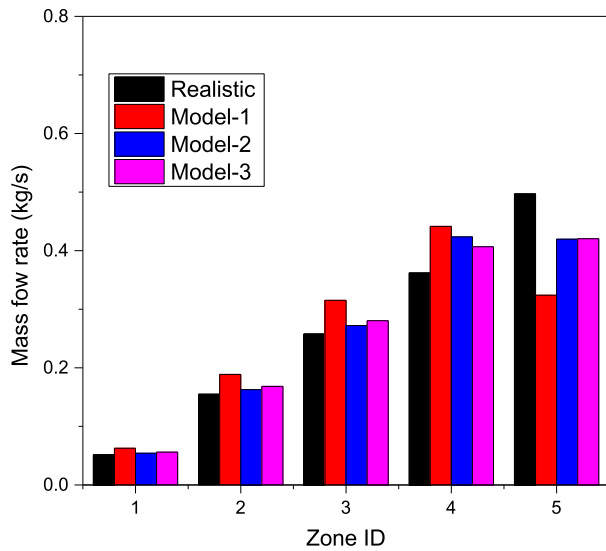


Fig. 6. Average Velocity distribution.

into five region in radial direction, as shown in.

Fig. 5. And the mass flow rate in each region for Realistic modeling, Model-2 and Model-3 are shown in Fig. 6. Realistic modeling, Model-1, Model-2 and Model-3 all predict a small velocity (less than the average velocity 1.5 m/s) in the center region. Moreover, the average velocity predicted by Realistic modeling is 1.455 m/s, while the value predicted by Model-2 and Model-3 is about 1.461 m/s.

Fig. 7 shows the temperature distribution contour at the outlet of IWF by different models. Since the center is far from fuel rods and holds the largest axial velocity, the temperature is lowest in the center, as shown in Fig. 7(a). Model-1 failed to reproduce the temperature distribution. Model-2 and Model-3 predict the temperature distribution similar to that predicted by Realistic modeling. However, Model-2 over predicted the maximum and minimum temperature by about 15K. While Model-3 under predicted these values with a maximum deviation of about 4K.

Fig. 8 shows the average, maximum and minimum temperature distribution along axial direction in IWF and AF. Since a uniform power distribution is assumed along the axial direction within AF, the average temperature should increase linearly along the axial direction. And this has been well predicted by different models, as

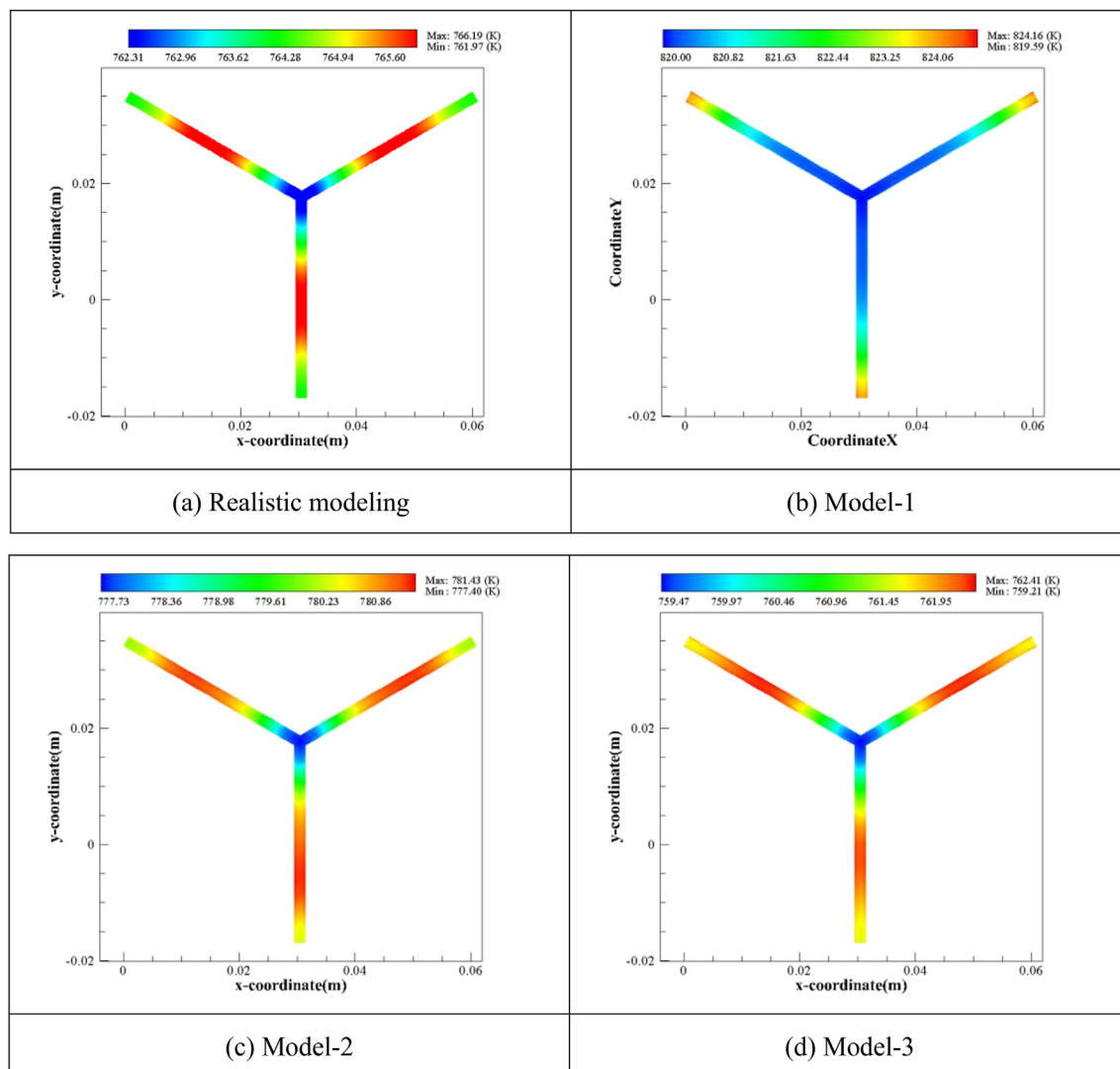


Fig. 7. Temperature distribution in IWF (Uniform power distribution).

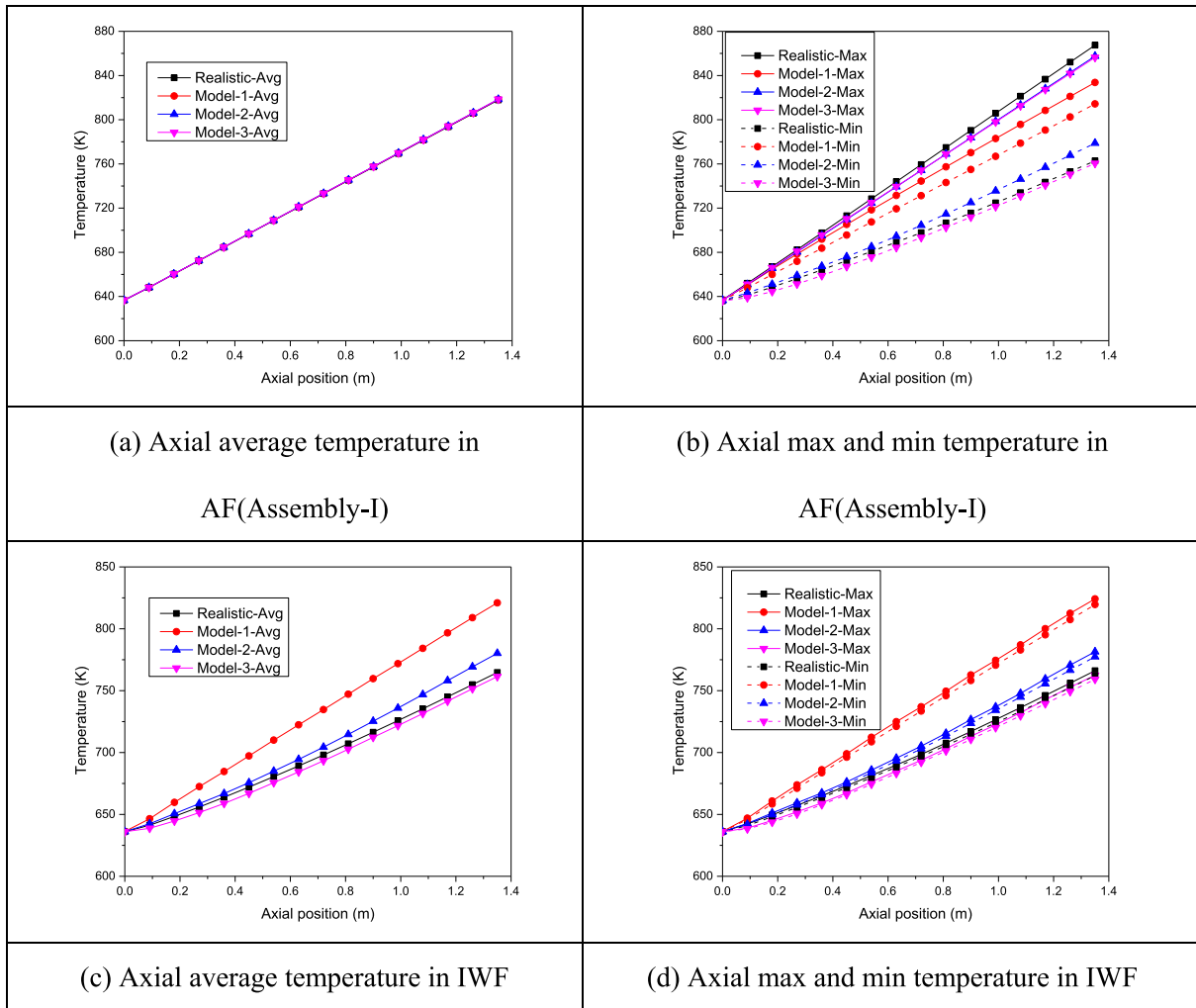


Fig. 8. Axial temperature distribution (Uniform power distribution).

shown by Fig. 8 (a). But when it comes to the maximum and minimum temperature distribution, predictions of three porous models show some difference to those predicted by Realistic modeling, as shown in Fig. 8 (b). In particular, all porous medium model under predict the maximum temperature and the discrepancy is accumulated along the flow direction. Model-2 has a closer minimum temperature prediction than Model-1, but the deviation is quite obvious when the elevation is larger than 0.6 m. The minimum temperature predicted by Model-3 has achieved excellent agreement with Realistic modeling. Fig. 8 (c) shows the axial average temperature distribution in IWF. At the entrance region near the duct inner-wall, the velocity is larger than that in lower region due to uniform velocity distribution assumption at the inlet. Therefore, less energy is transferred from the heat source to the duct wall at the entrance region, which leads to a lower radial heat transfer between the AF and IWF. As a consequence, the average temperature shows a slow increase at the entrance region. Realistic modeling, Model-2 and Model-3 have captured this phenomenon while Model-1 did not. After the entrance region, the average temperature predicted by Model-2 shows increasing discrepancy to that predicted by Realistic modeling, while Model-3 shows decreasing discrepancy. Fig. 8 (d) shows the maximum and minimum temperature distribution along axial direction in IWF. Model-3 shows the best prediction among three porous medium model.

Table 7 shows the total surface heat transfer through wall-6 of

Table 7

Key parameters at  $Pe = 174$ (Uniform power distribution).

Case ID	Total surface heat transfer(W)	Deviation (%)
Realistic	476.186	—
Model-1	684.5032	43.7
Model-2	536.9533	12.8
Model-3	465.149	−2.3

Assembly-I predicted by different models when the Peclet number  $Pe_p$  for AF is 174. Total surface transfer predicted by Model-1 and Model-2 show a serious overestimation and the relative deviations are 43.7% and 12.8%, respectively. While, Model-3 achieved a good agreement with Realistic modeling with a deviation of −2.3%.

### 3.1.2. Results at different Peclet number

Further simulation has been performed with different Peclet numbers to investigate the performance of these porous medium models. The inlet velocity for AF increases from 1.5 m/s to 7.00 m/s, while all other boundary conditions stay the same. More energy in AF is taken away by axial flow with the increased velocity, and less energy is transferred through duct wall in radial direction. In other words, total surface heat transfer through duct wall decrease with Peclet number. And the decrease has been well predicted, as shown in Fig. 9(a). Fig. 9(b) shows relative deviations of total surface heat



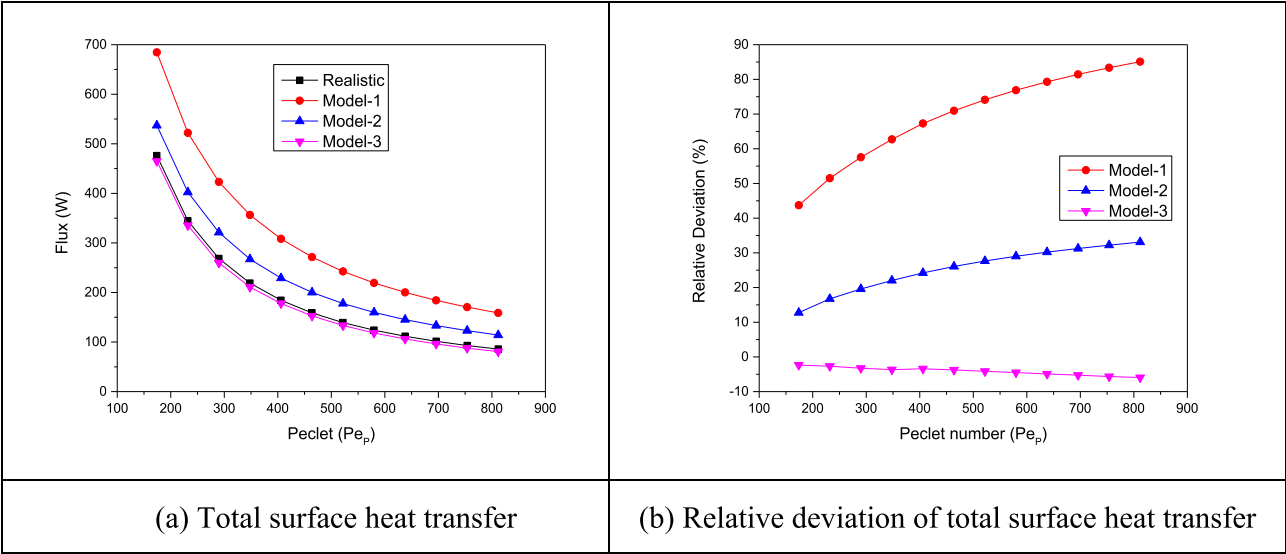


Fig. 9. Total surface heat transfer at different Peclet number (Uniform power distribution).

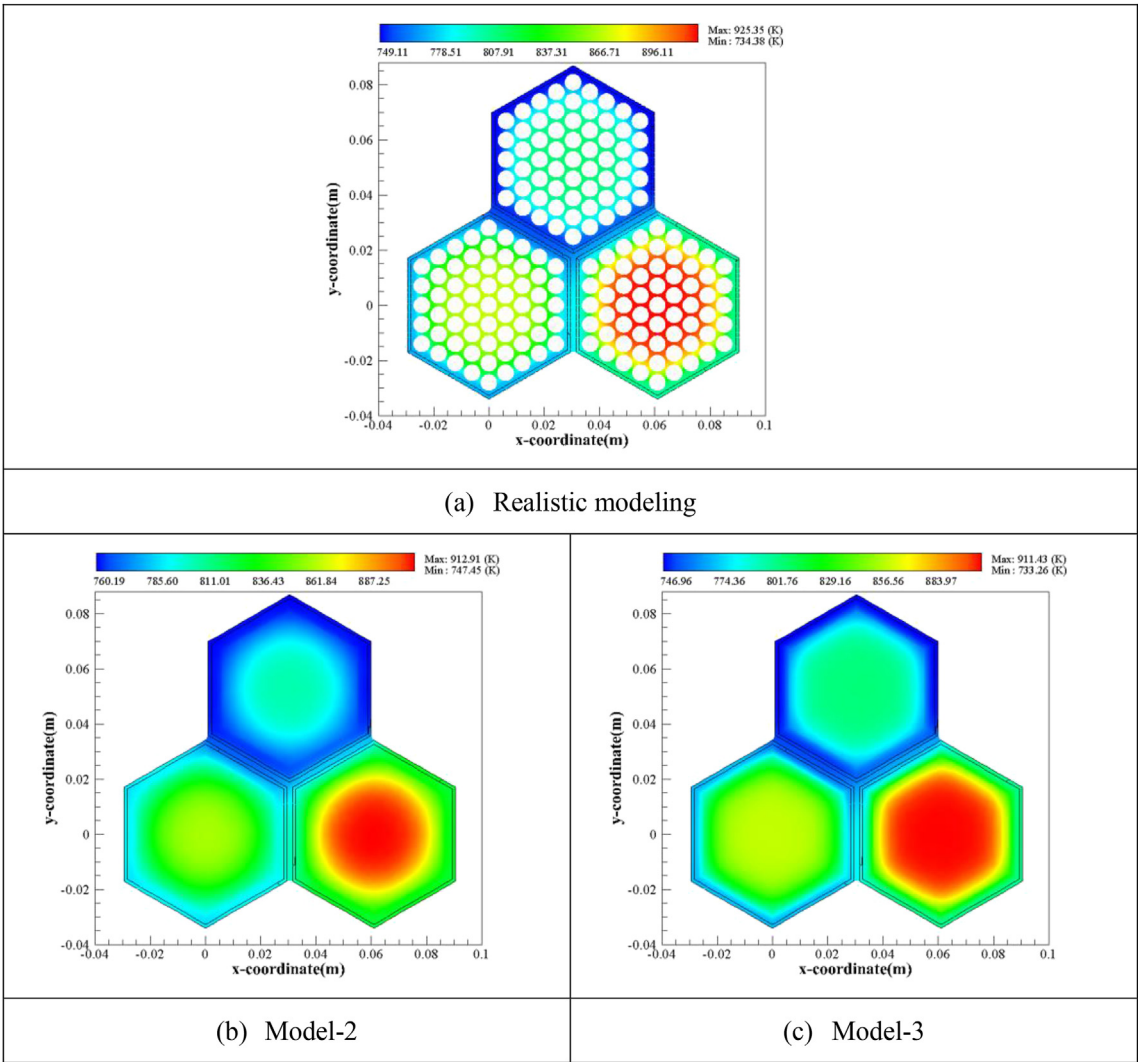


Fig. 10. Temperature at the outlet of AF (Non-Uniform power distribution).

transfer predicted by three porous medium models. The deviations for Model-1 and Model-2 are getting larger with the increase of Peclet number and the largest deviations reach 85.1% and 33.1%, respectively. While Model-3 is also getting larger, but the speed is much slower. The largest deviation for Model-3 is –6%.

### 3.2. Non-uniform power distribution

In present thermal mode, a non-uniform power distribution is assumed among three assemblies. The heat flux for fuel rods in Assembly-II is 25% larger than that for fuel rods in Assembly-I, while the heat flux for fuel rods in Assembly-III is 25% less. Since uniform porous medium Model-1 failed to predict the temperature distribution within AF, it will not be discussed in this section.

#### 3.2.1. Results at a given Peclet number = 174

Fig. 10 shows the temperature distribution contour predicted by different models at the outlet of assemblies. Compared to Assembly-I, the energy sources for Assembly-II and Assembly-III were changed by 20% and –20%, respectively. The temperature distribution at the outlet of three assembly is different to each other, as shown in Fig. 10 (a). Model-2 and Model-3 underestimate

the maximum temperature by 12.4K and 13.9K, respectively. And these deviations are almost the same with those in 3.1.1. Again, Model-3 well predicted the minimum temperature.

Fig. 11 shows the temperature distribution within IWF predicted by different models. And the temperature distribution is heavy influenced by neighbor assemblies. The minimum temperature point transferred from the center of IWF to the branch between two assemblies with lower temperature. The temperature ranges predicted by Model-3 is closer to the range predicted by Realistic modeling than the range predicted by Model-2.

Fig. 12(a)–(f) show the average, maximum and minimum temperature distribution along axial direction in AF and IWF. The performance of model-2 and model-3 is almost the same as in 3.1. And no obvious deterioration or improvement has been noticed. Further investigation on the temperature distribution in AF reveals that below the elevation of 0.6 m which is about the diameter for circumcircle of the duct inner wall, Model-2 predicts the average temperature distribution more accurate than Model-3. But Model-3 shows a better performance after the elevation of 0.6 m.

Table 8 shows the total surface heat transfer through duct of three assemblies predicted by different models when the Peclet number  $Pe_p$  for AF is 174. Wall-ID is shown in Fig. 1. For Wall-

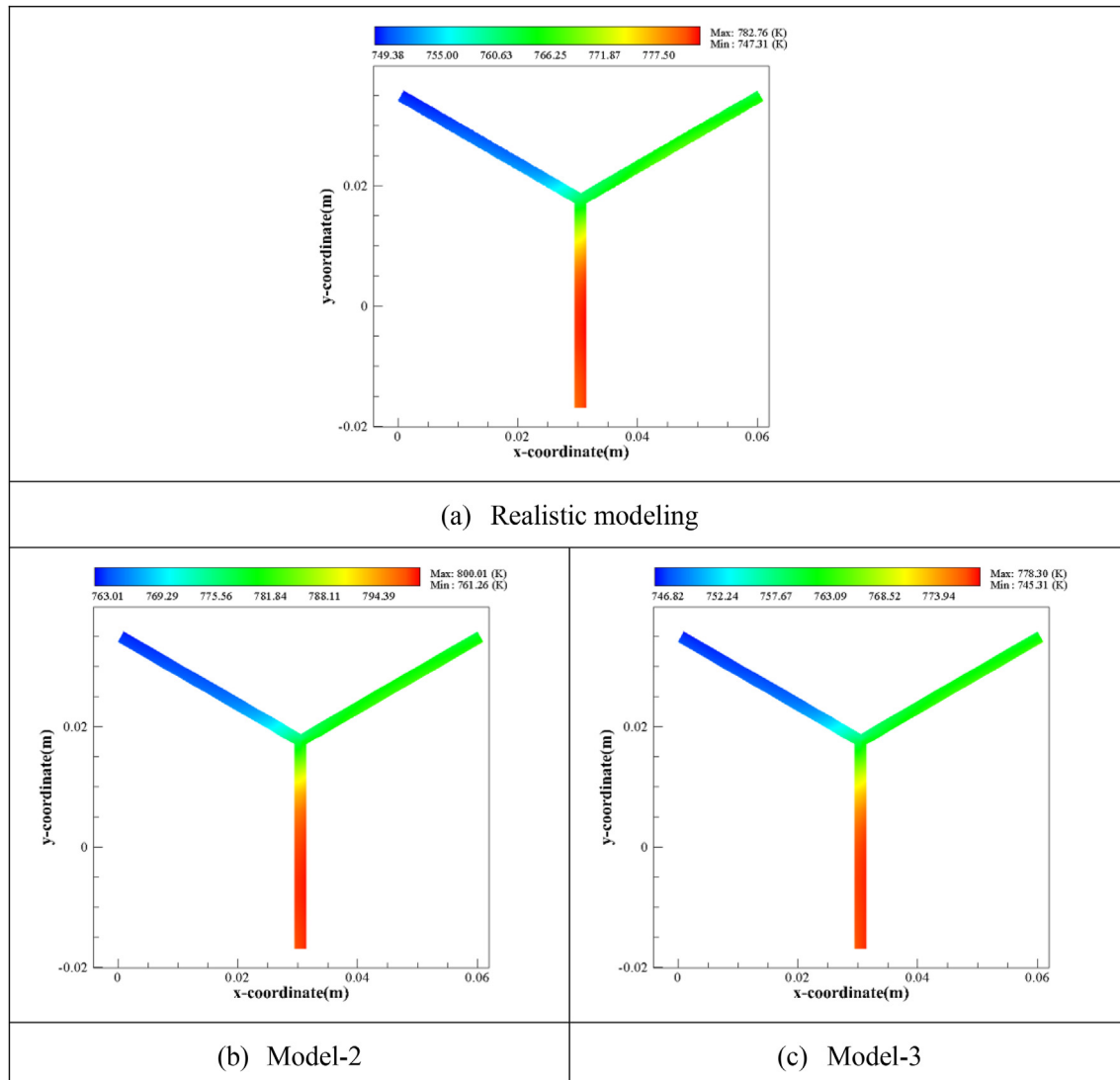
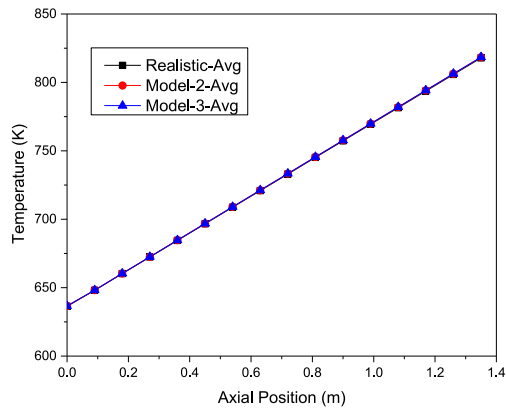
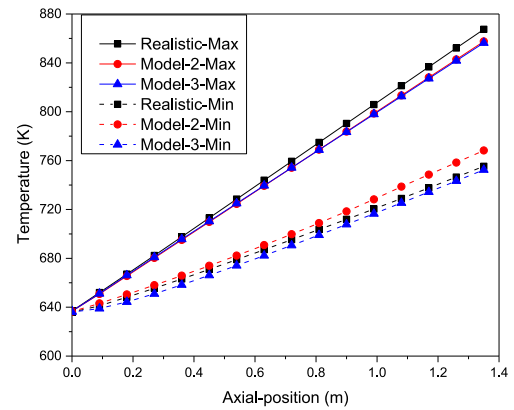


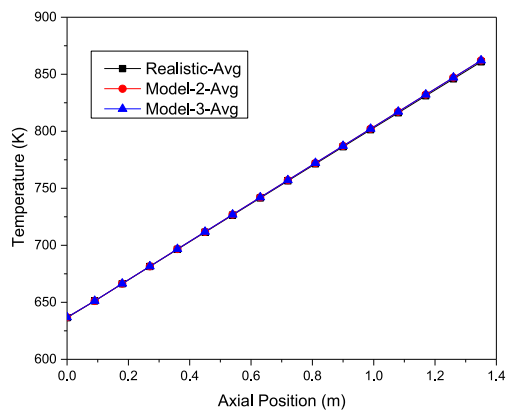
Fig. 11. Temperature Distribution in IWF (Non-Uniform power distribution).



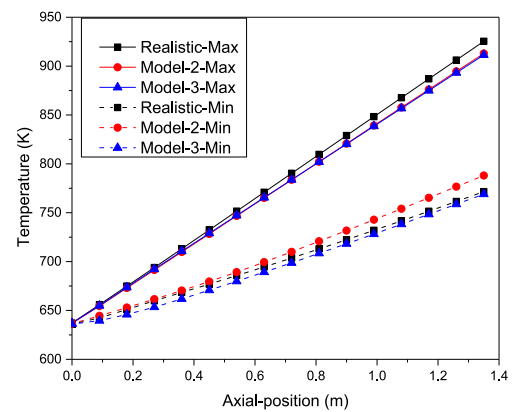
(a) Axial average temperature in  
AF(Assembly-I)



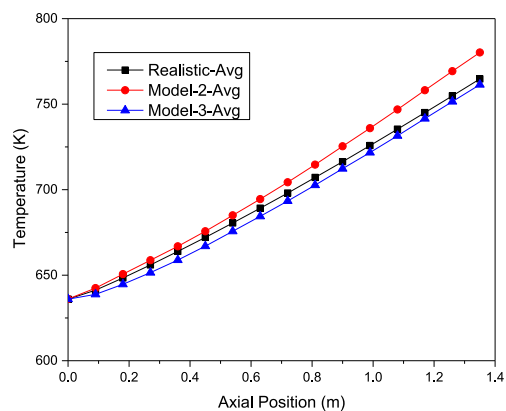
(b) Axial max and min temperature in  
AF(Assembly-I)



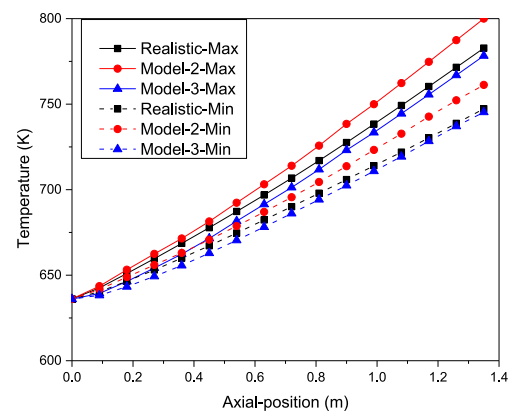
(c) Axial average temperature in  
AF(Assembly-II)



(d) Axial max and min temperature in AF  
(Assembly-II)



(e) Axial average temperature in IWF



(f) Axial max and min temperature in IWF

**Fig. 12.** Axial temperature distribution (Non-Uniform power distribution).

**Table 8**Key parameters at  $Pe = 174$  (Non-Uniform power distribution).

Wall-ID	Realistic modeling	Model-2		Model-3	
	Total surface heat transfer(W)	Total surface heat transfer(W)	Deviation (%)	Total surface heat transfer(W)	Deviation (%)
Wall-5(Assembly-I)	825.19	444.61	−46.12	714.98	−13.36
Wall-6(Assembly-I)	1793.02	1603.68	−10.56	1714.51	−4.38
Wall-1(Assembly-II)	3407.04	2967.72	−12.89	3198.39	−6.12
Wall-2(Assembly-II)	2091.73	1852.91	−11.42	1960.74	−6.26
Wall-3(Assembly-III)	1138.98	784.50	−31.12	858.13	−24.66
Wall-4(Assembly-III)	2462.16	1786.34	−27.45	1915.03	−22.22

5(Assembly-I), Wall-3(Assembly-III) and Wall-4(Assembly-III), heat is transferred from IWF to AF and the total surface heat transfer has been obviously underestimated on these surface. It is because the flow rate near the wall within AF is underestimated by porous medium model and less energy is taken away by axial flow. Since less energy is transferred from IWF to AF, the process of heat transfer from AF to IWF might be suppressed. Therefore, total surface heat transfer on all walls are underestimated in Table 8.

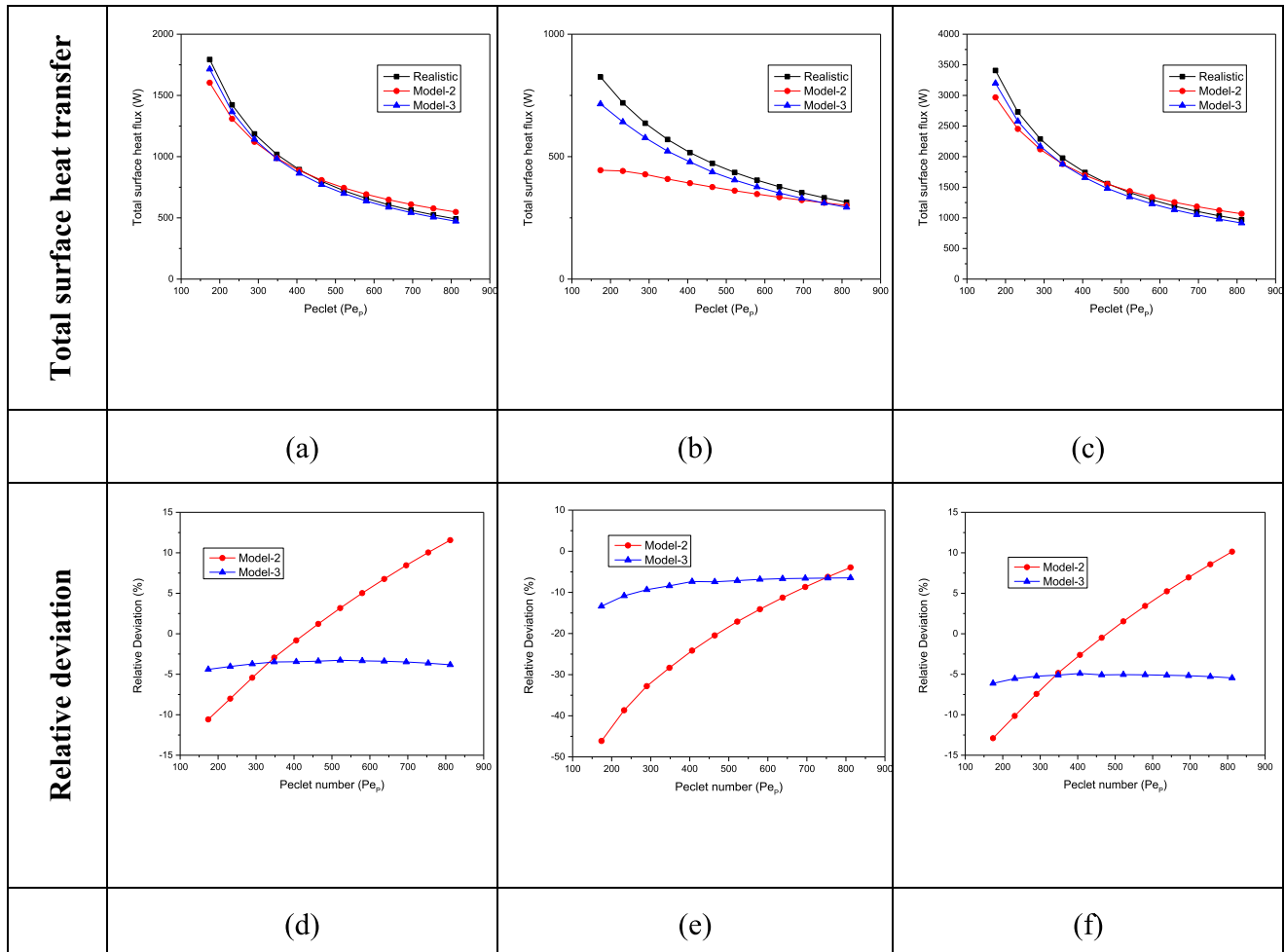
### 3.2.2. Results at different Peclet number

Fig. 13 shows the total surface heat transfer through three duct walls at different Peclet number. The heat transfer from AF to IWF is predicted well by porous medium models, as shown in Fig. 13 (a) and (c). In addition, the prediction deviation for Model-2 ranges

from −15% to 15% for Model-2, while it ranges from −6% to −3% for Model-3. For heat transfer from IWF to AF, the prediction shows larger deviation. In particular, the prediction deviation for Model-2 ranges from −46% to −3%, while it ranges from −13% to −6% for Model-3. Moreover, for Model-2, the prediction deviation for heat transfer from IWF to AF decrease with the increase of Peclet number and the prediction deviation for heat transfer from AF to IWF approaches the case in 3.1.2. It might be a confirmation of the explanation for Table 8.

## 4. Conclusion

Hybrid medium model has been proposed for predicting the conjugate heat transfer in the core of sodium-cooled fast reactor. To

**Fig. 13.** Total surface heat transfer at different Peclet number (Non-Uniform power distribution).

take into account the channel effect near the duct wall, the AF is divided into a porous medium region in the center and a pure fluid region filled with coolant in the peripheral.

Comparing with the Realistic modeling, hybrid medium model holds the advantage of saving computational cost as conventional porous medium models do. In addition, hybrid medium model shows an obvious improvement in prediction of temperature distribution within the inter-wrapper flow and the radial heat transfer and between the inter-wrapper flow and the assembly flow. In particular, the deviation for temperature distribution prediction has dropped from 16K to 3K. The deviation for radial heat transfer prediction is managed to achieve a reasonable accuracy with a maximum deviation of 15% while the maximum deviation for conventional porous medium model is 46%.

## Acknowledgements

The authors gratefully acknowledge the supports from Natural Science Foundation of China (Grant Nos. 11605131, 11705139 and 11675127) and K. C. Wong Education Foundation.

## References

- [1] D. Tencine, Some thermal hydraulic challenges in sodium cooled fast reactors, *Nucl. Eng. Des.* 240 (2010) 1195–1217.
- [2] N. Yue, D. Zhang, J. Chen, P. Song, X.a. Wang, S. Wang, S. Qiu, G. Su, Y. Zhang, The development and validation of the inter-wrapper flow model in sodium-cooled fast reactors, *Prog. Nucl. Energy* 108 (2018) 54–65.
- [3] D. Weinberg, K. Rust, H. Hoffmann, H. Hayafune, K. Hain, Transient neptun experiments on passive decay heat removal, in: *Proc. 3rd JSME/ASME Joint Int. Conf. On Nucl. Eng.*, Kyoto, Japan, 1995, pp. 519–524.
- [4] H. Kamide, K. Hayashi, T. Isozaki, M. Nishimura, Investigation of core thermohydraulics in fast reactors—interwrapper flow during natural circulation, *Nucl. Technol.* 133 (2001) 77–91.
- [5] M. Wang, Q. Zuo, H. Yu, W. Tian, G. Su, S. Qiu, Multiscale thermal hydraulic study under the inadvertent safety injection system operation scenario of typical pressurized water reactor, *Sci. Technol. Nucl. Install.* 2017 (2017).
- [6] E. Khan, W. Rohsenow, A. Sonin, N. Todreas, A porous body model for predicting temperature distribution in wire-wrapped fuel rod assemblies, *Nucl. Eng. Des.* 35 (1975) 1–12.
- [7] K. Basehore, N.E. Todreas, *Superenergy-2: A Multiassembly, Steady-State Computer Code for Lmfbr Core Thermal-Hydraulic Analysis*, Battelle Pacific Northwest Labs, Richland, WA (USA), 1980.
- [8] I. Maekawa, Numerical diffusion in single-phase multi-dimensional thermal-hydraulic analysis, *Nucl. Eng. Des.* 120 (1990) 323–339.
- [9] R. Hu, Y. Yu, A computationally efficient method for full-core conjugate heat transfer modeling of sodium fast reactors, *Nucl. Eng. Des.* 308 (2016) 182–193.
- [10] A. Gerschenfeld, S. Li, Y. Gorse, R. Lavastre, Development and validation of multi-scale thermal-hydraulics calculation schemes for sfr applications at cea, in: *Proceedings of the International Conference on Fast Reactors and Related Fuel Cycles: Next Generation Nuclear Systems for Sustainable Development*, Russian Federation, Yekaterinburg, 2017.
- [11] U. Parthasarathy, T. Sundararajan, C. Balaji, K. Velusamy, P. Chellapandi, S. Chetal, Decay heat removal in pool type fast reactor using passive systems, *Nucl. Eng. Des.* 250 (2012) 480–499.
- [12] Y. Yu, E. Merzari, A. Obabko, J. Thomas, A porous medium model for predicting the duct wall temperature of sodium fast reactor fuel assembly, *Nucl. Eng. Des.* 295 (2015) 48–58.
- [13] A. Kuznetsov, Analytical investigation of the fluid flow in the interface region between a porous medium and a clear fluid in channels partially filled with a porous medium, *Appl. Sci. Res.* 56 (1996) 53–67.
- [14] J.A. Ochoa-Tapia, S. Whitaker, Heat transfer at the boundary between a porous medium and a homogeneous fluid, *Int. J. Heat Mass Transf.* 40 (1997) 2691–2707.
- [15] M.J. de Lemos, R.A. Silva, Turbulent flow over a layer of a highly permeable medium simulated with a diffusion-jump model for the interface, *Int. J. Heat Mass Transf.* 49 (2006) 546–556.
- [16] J. Chen, D. Zhang, P. Song, X. Wang, S. Wang, Y. Liang, S. Qiu, Y. Zhang, M. Wang, G. Su, Cfd investigation on thermal-hydraulic behaviors of a wire-wrapped fuel subassembly for sodium-cooled fast reactor, *Ann. Nucl. Energy* 113 (2018) 256–269.
- [17] K. Rehme, The structure of turbulent flow through rod bundles, *Nucl. Eng. Des.* 99 (1987) 141–154.
- [18] F. Kuwahara, Y. Kameyama, S. Yamashita, A. Nakayama, Numerical modeling of turbulent flow in porous media using a spatially periodic array, *J. Porous Media* 1 (1998).
- [19] M.J. De Lemos, *Turbulence in Porous Media: Modeling and Applications*, Elsevier, 2012.
- [20] J. Mahaffy, B. Chung, C. Song, F. Dubois, E. Graffard, F. Ducros, M. Heitsch, M. Scheuerer, M. Henriksson, E. Komen, *Best Practice Guidelines for the Use of Cfd in Nuclear Reactor Safety Applications*, Organisation for Economic Co-Operation and Development, 2007.
- [21] Y. Yu, et al., Merzari E, Obabko A, A porous medium model for predicting the duct wall temperature of sodium fast reactor fuel assembly, *Nucl. Eng. Des.* 295 (2015) 48–58.